

# Computation-Guided Placement of Nonfullerene Acceptor Core Halogenation for High-Performance Organic Solar Cells

Yao Chen,\*<sup>#</sup> Hongliang Lei,<sup>#</sup> Seunglok Lee, Peihao Huang, Gengsui Tian, Lei Liu, Tianyu Zeng, Changduk Yang, Tainan Duan, Huanyu Zhou, Zeyun Xiao,\* Tobin J. Marks,\* and Antonio Facchetti\*



Cite This: <https://doi.org/10.1021/jacs.5c16058>



Read Online

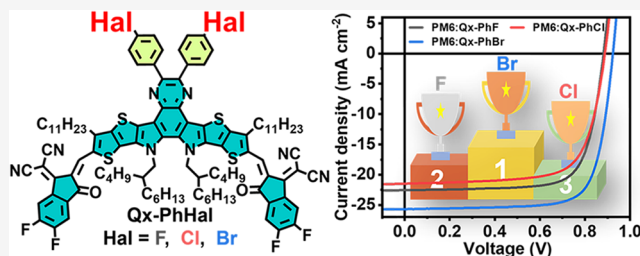
ACCESS |

Metrics & More

Article Recommendations

Supporting Information

**ABSTRACT:** The strategic molecular design of nonfullerene acceptors (NFAs) plays a crucial role in enhancing the efficiency of organic solar cells (OSCs). Here, working from first-principles theoretical computation, we report a new series of quinoxaline-based NFAs ( $\text{Qx-PhHal}$ , where  $\text{Hal} = \text{F}, \text{Cl}$ , or  $\text{Br}$ ) with varying halogen substitution on the central acceptor core of the molecules to investigate their impact on OSC performance. Notably, OSCs incorporating the brominated NFA demonstrate a significantly higher power conversion efficiency (PCE = 17.58%) than those with fluorinated or chlorinated NFAs (~14%). Theoretical and experimental analyses reveal that bromination enhances electrostatic interactions, donor–acceptor miscibility, crystallinity, and fibrillar film morphology versus the other halogenated NFAs, thereby enhancing exciton dissociation efficiency, more balanced hole/electron mobility, and reduced exciton recombination rates in the corresponding OSCs. Additionally, ternary solar cells incorporating the brominated NFA as the third component achieve a very high PCE of 20.14%. These findings provide valuable insights into the molecular design of future high-performance NFAs for OSC applications.



## INTRODUCTION

Organic solar cells (OSCs) have garnered considerable research interest for next-generation renewable energy technologies owing to their straightforward scalable solution processability, lightweight, mechanical flexibility, and the absence of toxic heavy metals.<sup>1–5</sup> Enhancing OSC efficiency has relied on the development of new photoactive materials, innovations in thin-film processing techniques, optimization of device architectures, as well as via fine-tuning of the photoactive blend morphology.<sup>6–12</sup> Through these innovations, the past decade has witnessed striking progress in OSC power conversion efficiency (PCE), now exceeding 20% mainly through the discovery and optimization of third-generation nonfullerene acceptors (NFAs), especially the development of ITIC, IT-4F, and Y6.<sup>13–26</sup> Among them, NFAs of the Yn series (Figure 1a) exhibit strong light absorption in the visible–near-infrared (vis–NIR) region, tunable energy levels, excellent charge transport properties, and facile structural modifications, which are key factors for increasing the OSC efficiency.<sup>27–30</sup> Nevertheless, despite extensive efforts to rationally design NFAs, new approaches to control intermolecular interactions and film morphology, thereby effectively enhancing the PCE by balancing the trade-offs between open-circuit voltage ( $V_{\text{OC}}$ ), short-circuit current density ( $J_{\text{SC}}$ ), and fill factor (FF) remains of major interest, yet incompletely explored.<sup>31,32</sup>

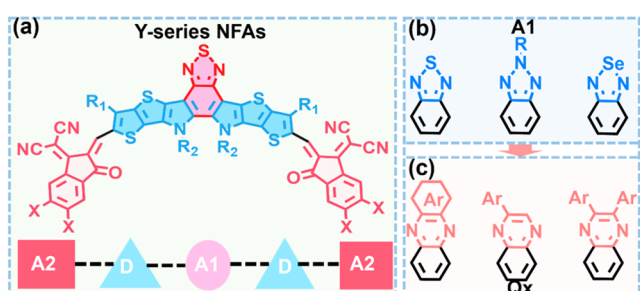


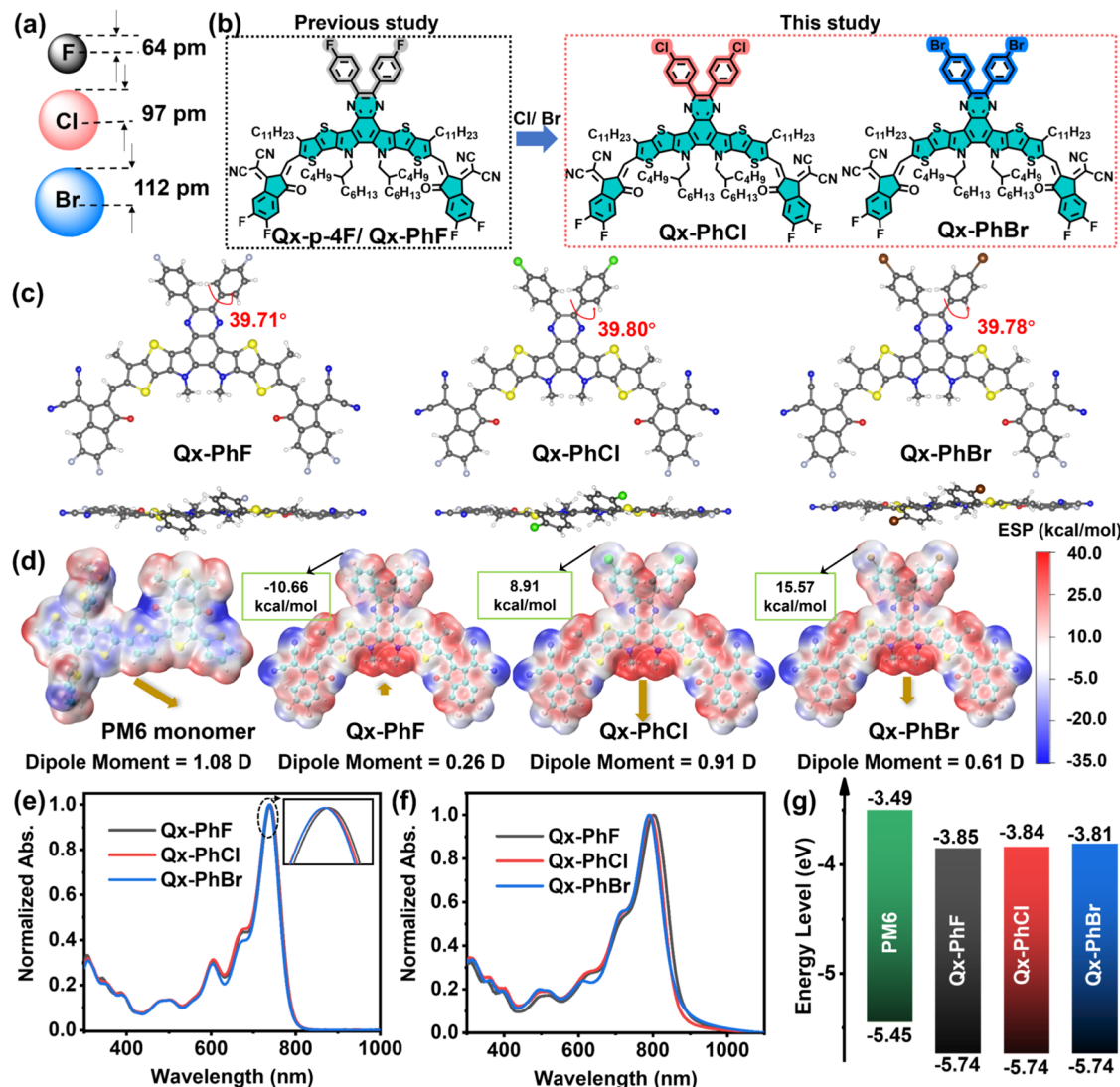
**Figure 1.** (a) Chemical structure of Y-series NFAs and (b, c) the development of A1 moiety structures reported in the literature.

The Y-series NFAs typically feature an electron-deficient central core, electron-rich donor units, electron-deficient terminal units, and side chains arranged in an acceptor–donor–acceptor–donor–acceptor (A2–D–A1–D–A2) configuration (Figure 1a).<sup>33,34</sup> Various strategies have been employed to improve the optoelectronic properties of NFAs, including modification of the central subunits, optimization of

Received: September 13, 2025

Revised: December 2, 2025

Accepted: December 23, 2025

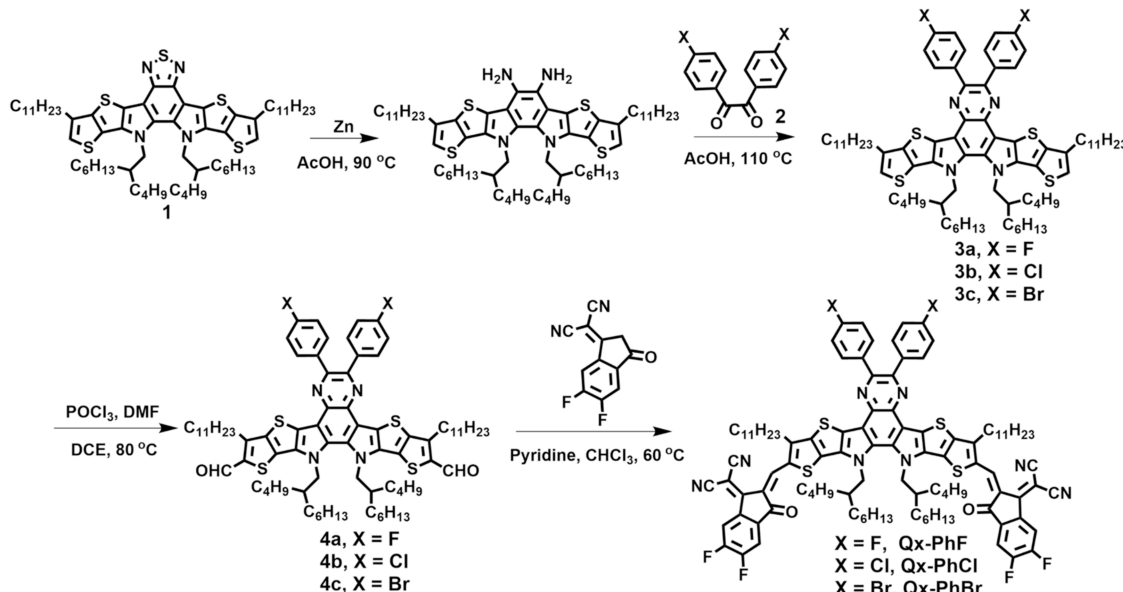


**Figure 2.** (a) Comparison of halogen atomic radii, (b) chemical structures of Qx-PhF, Qx-PhCl, and Qx-PhBr, (c) DFT-derived molecular structures, (d) electrostatic potential (ESP) and dipole moments of Qx-PhHal. (e) UV-vis spectra of the indicated NFAs in dilute solution, (f) in the thin-film state, and (g) energy-level diagrams of PM6 and the indicated NFAs.

the acceptor end groups, and engineering the side chains.<sup>35–38</sup> Among these design approaches, NFA halogenation (e.g., fluorination and chlorination) of various NFA constituents has been particularly effective in enhancing the OSC performance via a combination of electronic and structural packing effects. However, previous halogenation efforts of Y-series NFAs have predominantly focused on the end groups due to the limited functionalization sites on the central (A1) benzothiadiazole core unit (Figure 1b).<sup>39,40</sup> Importantly, end-group halogenation of benzothiadiazole-centered NFAs, such as those of the Yn family, has shown that F/Cl substitution invariably outperforms its brominated counterparts. For instance, the PCE with various donors of Y6 (X = F) and BTP-eC11 (X = Cl) ranges 15–19% while those of TPIC-4Br (X = Br) are 7–14%, suggesting that Br functionalization does not result in high-performing NFAs.<sup>33,41–44</sup> Therefore, the state-of-the-art NFAs have widely adopted fluorinated and chlorinated end groups limiting exploration of Br-substituted NFAs.<sup>41,45,46</sup> Halogenation at the central unit of NFA is very limited with one study suggesting that chlorination outperforms all other types of halogenation<sup>46</sup> while another suggesting that it is

equivalent to bromination;<sup>47</sup> however, the latter study did not include fluorination. Thus, it remains unclear whether the effect of end-group versus core halogenation differs and whether bromination always underperforms the other halogenation strategies.

Recently, quinoxaline-based (Qx) fused cores have been incorporated into NFA central units (A1) to further improve OSC PCEs (Figure 1c). These cores offer additional versatile functionalization handles, enabling greater flexibility in optimizing energy levels, enhancing intermolecular interactions, and fine-tuning of blend morphology.<sup>48–52</sup> Indeed, the introduction of the halogens into the Qx-based core has been successful in modifying NFA energy levels and fine-tuning the film morphology, ultimately improving OSC PCE.<sup>47,53</sup> Recently, Xie et al. investigated the effects of Qx core fluorination position (ortho, meta, and para) on molecular packing and photovoltaic performance.<sup>54</sup> The para-substituted acceptor (Qx-p-4F) shows favorable molecular stacking and, ultimately, higher PCE, providing an alternative avenue for constructing high-performance NFAs. Nevertheless, the role of halogens and the systematic comparison in modulating

**Scheme 1.** Synthetic Routes to Qx-PhHal Acceptors

electrostatic interactions, morphology, and photovoltaic response of NFAs remains unresolved.<sup>47,51</sup>

Encouraged by the success of **Qx-p-4F**, in this contribution, we systematically design, synthesize, characterize, and incorporate in OSCs, a new series of NFAs (**Qx-PhHal**) with varied halogen substitution (Hal = F → Cl → Br) on the phenyl groups attached to the central Qx core to address the role of halogen identity in modulating electrostatic interactions, molecular packing, film morphology, optoelectronic properties, and ultimately the photovoltaic response. The Qx platform enables central-core functionalization that is inaccessible in the widely studied Y series. Here, we specifically investigate how halogen substitution in Qx-based NFAs, while maintaining the end-group halogenation constant, affects structure–property–performance relationships, and whether these trends mirror those reported for Y-series and related NFAs, where F and Cl substitution typically outperform Br.<sup>53,55–60</sup> Our parallel theoretical calculations suggest that the halogen atoms on the central quinoxaline core have a minimal impact on the individual molecular geometries. However, the dipole moment orientations invert, and the electrostatic potential (ESP) of the halogen sites gradually turns positive on traversing from fluorine to chlorine/bromine, which promotes intermolecular interactions. The optical absorption spectra exhibit a slight blue shift when halogenating from F to Br, accompanied by elevated LUMO levels. Interestingly and unexpectedly, the morphology of the PM6:Qx-PhHal OSC blends is modulated by varying the halogen atoms, with bromination affording the most favorable nanofibrillar morphology for charge transport and thereby promoting the highest OSC performance. Consequently, due to the simultaneous enhancement in  $V_{OC}$ ,  $J_{SC}$ , and FF, the brominated PM6:Qx-PhBr blend exhibits a PCE of 17.58%, far higher than that of the fluorinated PM6:Qx-PhF or chlorinated PM6:Qx-PhCl blends (PCE ≈ 14%). Importantly, compared to traditional end-group halogenation in other NFAs,<sup>33,41,42,46,47</sup> an inverse performance trend is observed here, demonstrating that Br can afford more efficient cell performance than the corresponding F/Cl functionalized NFAs. Furthermore, by leveraging the aforementioned advantages, ternary OSCs that incorporate the Qx-

PhBr NFA as the third component in PM6:BTP-eC9 devices achieve an impressive PCE of 20.14%. This work highlights the critical role of NFA central-core halogenation in regulating electrostatic interactions and OSC film morphology while revealing an inverse trend in NFA halogenation, thereby providing valuable insights into future molecular design of high-performance NFAs.

## RESULTS AND DISCUSSION

### DFT Computations

To gain structural information, density functional theory (DFT) calculations at the B3LYP/6-31G(d,p) level were performed for the **Qx-PhHal** NFAs prior to their synthesis. From the optimized geometries (Figures 2 and S1–S3), the NFA conjugated backbone is planar with minimal variations upon halogen changes, with the dihedral angles between the halogenated phenyl ring and the Qx core being 39.71, 39.80, and 39.77° for **Qx-PhF**, **Qx-PhCl**, and **Qx-PhBr**, respectively. These comparable dihedral angles and identical backbone planarities for these NFAs suggest that halogen atoms in the para-position have negligible effects on the molecular structure.

To further evaluate the electronic effects, the ESP distributions and dipole moments of the NFAs were computed and compared. The quantified ESP area distribution and overall average ESP ( $ESP_{avg}$ ) values of the NFA compounds are summarized in Figure S3 and Table S1. Thus, on going from **Qx-PhF**, to **Qx-PhCl**, to **Qx-PhBr**, the ESP area distribution shifts slightly toward the positive direction, leading to an increase in  $ESP_{avg}$  from 5.15 to 5.42 to 5.28 kcal mol<sup>-1</sup>, respectively. Considering that most donor polymers have a negative  $ESP_{avg}$  e.g., -0.89 kcal mol<sup>-1</sup> for **PM6**,<sup>61</sup> replacing F with Cl/Br in **Qx-PhHal** enhances the electrostatic potential difference with the donor polymer, thereby strengthening donor–acceptor intermolecular interactions.<sup>3</sup> Additionally, the ESP value of the halogen becomes progressively more positive on going from F to Cl and Br, providing more effective interaction sites with the donor polymer. Furthermore, the **Qx-PhHal** dipole moment gradually increases from 0.26 D (**Qx-PhF**) to 0.91 D (**Qx-PhCl**) to 0.61 D (**Qx-PhBr**), respectively,

**Table 1.** Optoelectronic Parameters of Qx-PhF, Qx-PhCl, and Qx-PhBr

NFAs	dipole moment (Deybe)	$\lambda_{\text{sol}}^{\text{sol}}$ (nm)	$\lambda_{\text{max}}^{\text{film}}$ (nm)	$E_g^{\text{opta}}$ (eV)	$E_{\text{OX}}$ (V)	$E_{\text{RE}}$ (V)	$E_{\text{HOMO}}^b$ (eV)	$E_{\text{LUMO}}^b$ (eV)
Qx-PhF	0.26	739	802	1.38	0.94	-0.95	-5.74	-3.85
Qx-PhCl	0.91	738	792	1.39	0.94	-0.96	-5.74	-3.84
Qx-PhBr	0.61	737	790	1.40	0.94	-0.99	-5.74	-3.81

<sup>a</sup>Calculated from the empirical formula:  $E_g = 1240/\lambda_{\text{onset}}$ . <sup>b</sup>Estimated from cyclic voltammetry.

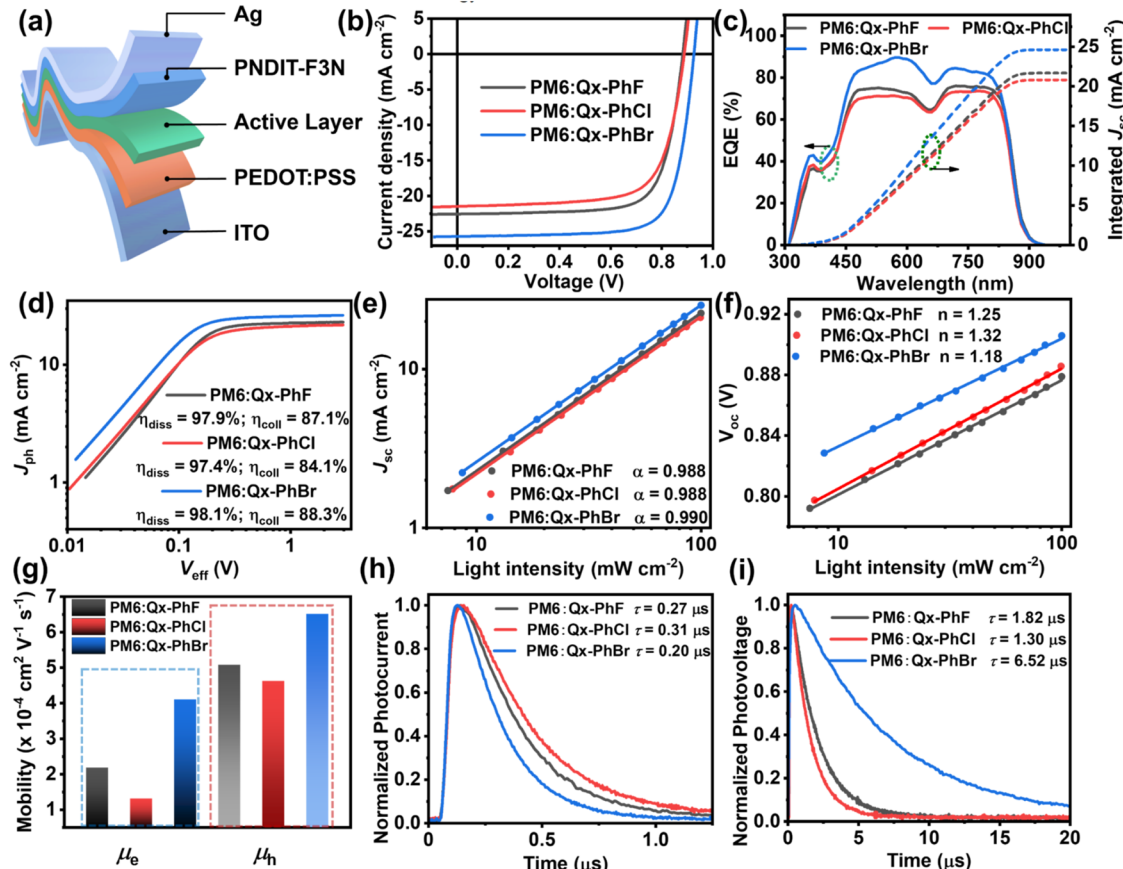


**Figure 3.** (a) Device architecture of the indicated OSCs characterized in this study; (b)  $J$ – $V$  and (c) EQE curves of the indicated devices; (d)  $J_{\text{ph}}$  versus  $V_{\text{eff}}$  plots; (e)  $J_{\text{sc}}$  versus light intensity; (f)  $V_{\text{oc}}$  versus light intensity; (g) electron and hole mobilities; (h) transient photocurrent; and (i) transient photovoltage of PM6:Qx-PhF, PM6:Qx-PhCl, and PM6:Qx-PhBr devices.

with reversed dipole moment orientation when replacing F with Cl or Br. The enhanced dipole moment is expected to facilitate more efficient charge dissociation (*vide infra*).

### Synthesis and Characterization

The syntheses of Qx-PhF, Qx-PhCl, and Qx-PhBr are presented in **Scheme 1**. Detailed characterization of all compounds can be found in the **Supporting Information** and includes <sup>1</sup>H NMR and MS analysis. The thermal properties of Qx-PhHal NFAs were investigated by differential scanning calorimetry (DSC) and thermogravimetric analysis (TGA) (**Figure S4**). These new NFAs exhibit high thermal stability with decomposition temperature onsets ( $T_d$ ) of 323, 318, and 328 °C for Qx-PhF, Qx-PhCl, and Qx-PhBr, respectively, as assessed by TGA. Furthermore, the DSC measurements reveal that the brominated Qx-PhBr has a higher melting transition temperature ( $T_m = 286$  °C) compared to Qx-PhF ( $T_m = 223$  °C) and Qx-PhCl ( $T_m = 271$  °C).

UV-vis absorption spectra of the present NFAs in dilute chloroform solution and as thin films are shown in **Figure 2e,f**, and the optical data are summarized in **Table 1**. The Qx-PhF,

Qx-PhCl, and Qx-PhBr optical absorption profiles in solution are almost identical and exhibit only a slightly blue-shifted absorption peak maxima ( $\lambda_{\text{Max}}^{\text{sol}}$  739, 738, and 737 nm, respectively). Going from solution to the solid state, all NFAs exhibit a red-shifted absorption (~43 nm) with a  $\lambda_{\text{Max}}^{\text{film}}$  of 802, 792, and 790 nm for Qx-PhF, Qx-PhCl, and Qx-PhBr, respectively, similar to the trend in the solution state. Overall, all NFA exhibit almost identical absorption spectra in solution, while that of the Qx-PhBr thin film is slightly blue-shifted compared to that of the Qx-PhF one, which may be attributed to the weaker  $\pi$ – $\pi$  stacking in the solid state (*vide infra*). The optical band gaps ( $E_g^{\text{opt}}$ ) assessed from the onset of thin-film absorption spectra are 1.38, 1.39, and 1.40 eV for Qx-PhF, Qx-PhCl, and Qx-PhBr, respectively. These results reveal that reducing the electronegativity of the halogen atom (F → Br) slightly enlarges the band gap. Thin-film cyclic voltammetry (CV) measurements were next conducted to assess the redox properties and thus the highest occupied molecular orbital (HOMO) and lowest unoccupied molecular orbital (LUMO) energy levels of the newly synthesized NFAs (**Figures S5** and

**Table 2.** Photovoltaic Metrics of PM6:Qx-PhF, PM6:Qx-PhCl, and PM6:Qx-PhBr OSCs

active layer	$V_{OC}$ (V)	$J_{SC}$ (mA/cm <sup>2</sup> )	$J_{Cal}^{EQE^a}$ (mA/cm <sup>2</sup> )	FF (%)	PCE (%) <sup>b</sup>
PM6:Qx-PhF	0.88 (0.88 ± 0.002)	22.56 (22.46 ± 0.23)	21.68	74.22 (73.10 ± 0.79)	14.77 (14.45 ± 0.20)
PM6:Qx-PhCl	0.89 (0.89 ± 0.002)	21.49 (21.19 ± 0.29)	20.80	71.21 (71.48 ± 0.78)	13.59 (13.42 ± 0.15)
PM6:Qx-PhBr	0.91 (0.91 ± 0.004)	25.59 (25.32 ± 0.49)	24.61	75.53 (75.13 ± 0.74)	17.58 (17.20 ± 0.25)

<sup>a</sup> $J_{Cal}^{EQE}$  obtained from the integration of the EQE. <sup>b</sup>Average parameters calculated from 10 devices.

2f). Details are reported in the Supporting Information. Based on the oxidation and reduction onset potentials, the HOMO/LUMO energy levels of Qx-PhF, Qx-PhCl, and Qx-PhBr were determined to be -5.74/-3.85, -5.74/-3.84, and -5.74/-3.81 eV, respectively. Interestingly, while Qx-PhF, Qx-PhCl, and Qx-PhBr have comparable HOMO energies, similar to the trend found from DFT computations, a noticeable upward shift in the LUMO level is observed going from Qx-PhF to Qx-PhCl to Qx-PhBr as the halogen electron-withdrawing ability gradually weakens going from F to Cl to Br, which in principle could raise the  $V_{OC}$  of the corresponding OSC. Overall, the energy levels of Qx-PhF, Qx-PhCl, and Qx-PhBr are well-aligned with those of the PM6 donor polymer, which was selected for OSC fabrication.

### OSC Fabrication and Performance Evaluation

OSCs were fabricated with the conventional architecture of ITO/PEDOT:PSS/PM6:Qx-PhF, Qx-PhCl, or Qx-PhBr/PNDIT-F3N/Ag (Figure 3a). The optimal thickness of the photoactive layer is approximately 100 nm. As shown in Tables 2 and S2–S4, the optimized PM6:Qx-PhBr blend OSCs deliver a PCE of 17.58% ( $V_{OC}$  = 0.91 V,  $J_{SC}$  = 25.59 mA cm<sup>-2</sup>, FF = 75.53%), significantly higher than those of PM6:Qx-PhF (PCE = 14.77%,  $V_{OC}$  = 0.88 V,  $J_{SC}$  = 22.56 mA cm<sup>-2</sup>, FF = 74.22%) and PM6:Qx-PhCl (PCE = 13.59%,  $V_{OC}$  = 0.89 V,  $J_{SC}$  = 21.49 mA cm<sup>-2</sup>, FF = 71.21%). Note, all device metrics ( $V_{OC}$ ,  $J_{SC}$ , and FF) are simultaneously elevated with the brominated NFA. Thus, in this family an opposite trend in the effect of halogenation is observed compared to traditional end-group halogenated NFAs.<sup>62</sup> The slightly higher  $V_{OC}$  of the device utilizing Qx-PhBr is attributed to the elevated LUMO energy level. Furthermore, the enlarged  $J_{SC}$  and FF highly correlate with weaker charge recombination and favorable film morphology (*vide infra*).<sup>63</sup> As shown in Figure 3c, a similar photoresponse (EQE) is observed for all three blends, which is consistent with the absorption spectra of those blends (Figure 2f). However, the photon-to-electron response intensity of the PM6:Qx-PhBr cells is much higher than those of PM6:Qx-PhF and PM6:Qx-PhCl, with a maximum EQE of 89.7% at 580 nm. The higher integrated current of 24.61 mA cm<sup>-2</sup> (within 5% error) for PM6:Qx-PhBr vs 21.68 mA cm<sup>-2</sup> for PM6:Qx-PhF and 20.80 mA cm<sup>-2</sup> for PM6:Qx-PhCl are aligned with the measured  $J_{SC}$ . Furthermore, the thermal stability of these OSCs was recorded at 80 °C. As shown in Figure S9, the  $T_{80}$  values (the time needed to reach 80% of the initial PCE) for PM6:Qx-PhF, PM6:Qx-PhCl, and PM6:Qx-PhBr OSCs are 263, 254, and 310 h, respectively, demonstrating that bromination also enhances thermal stability in the devices. Additionally, all OSCs exhibit comparable shelf-storage and light stability (Figure S10).

### Comparative Analysis of Charge Recombination, Exciton Dissociation, and Charge Transport Properties

Charge generation efficiency was studied by measuring the photocurrent density ( $J_{ph}$ ) versus the effective voltage ( $V_{eff}$ ) (Figure 3d).<sup>64,65</sup> Thus, the efficiency of exciton dissociation

( $\eta_{diss}$ ) of the PM6:Qx-PhBr solar cells is slightly larger than that of the other two blends, with  $\eta_{diss}$  values of 97.9%, 97.4%, and 98.1% for PM6:Qx-PhF, PM6:Qx-PhCl, and PM6:Qx-PhBr, respectively. Similarly, the efficiency of charge collection ( $\eta_{coll}$ ) of the PM6:Qx-PhBr OSCs is greater than that of the other two blends with  $\eta_{coll}$  values of 87.1, 84.1, and 88.3% for PM6:Qx-PhF, PM6:Qx-PhCl, and PM6:Qx-PhBr, respectively. The greater  $\eta_{diss}$  and  $\eta_{coll}$  in the PM6:Qx-PhBr blend indicates that the exciton dissociation and charge collection are greatly enhanced by central-core bromination, thereby elevating the PCE of the OSC.<sup>66</sup>

Furthermore, light intensity ( $I$ ) dependent  $J$ – $V$  analysis of the devices was next carried out to investigate bimolecular recombination. Typically, the relationship between  $J_{SC}$  and  $I$  is expressed as  $J_{SC} \propto I^\alpha$ , where the  $\alpha$  value represents the efficiency of bimolecular recombination.<sup>67,68</sup> A value of 1 for  $\alpha$  suggests the absence of bimolecular recombination loss.<sup>28,69</sup> Interestingly, all blends exhibit a comparable  $\alpha$  of 0.99, indicating the absence of bimolecular recombination in these halogenated NFA blends (Figure 3e). The reduced bimolecular recombination in the PM6:Qx-PhBr blend correlates with its higher FF of 75.53% than others. To obtain deeper insight into other OSC recombination processes, the  $I$ -depended  $V_{OC}$  was evaluated, which is governed by the relation  $V_{OC} = n \times (k_B T/e) \times \ln(I) + C$ , where  $n$  is the ideality constant,  $k_B$  is the Boltzmann constant,  $T$  is the temperature,  $e$  is the elementary charge, and  $C$  is a constant.<sup>69,70</sup> A smaller slope (close to 1.0  $k_B T/e$ ) indicates reduced monomolecular recombination in OSCs, typically associated with suppressed trap-assisted recombination.<sup>71</sup> The extracted  $n$  values were found to be 1.25, 1.32, and 1.18 for PM6:Qx-PhF, PM6:Qx-PhCl, and PM6:Qx-PhBr, respectively, indicating that the PM6:Qx-PhBr blend effectively suppresses the trap-assisted recombination (Figure 3f). This finding demonstrates that central-core halogenation engineering of Qx-PhHal NFAs strongly affects bimolecular recombination and trap-assisted charge recombination with the brominated central core more efficiently suppressing charge recombination.

Charge transport is another critical property connected with PCE variations.<sup>4</sup> Therefore, the blend hole and electron<sup>72–74</sup> mobilities of the blend were measured using the space–charge-limited current (SCLC) method<sup>75</sup> (Figures 3g and S11) with all values summarized in Table S4. The PM6:Qx-PhBr blend film exhibits a higher hole mobility ( $\mu_h$ ) of  $6.51 \times 10^{-4}$  cm<sup>2</sup> V<sup>-1</sup> s<sup>-1</sup> and electron mobility ( $\mu_e$ ) of  $4.10 \times 10^{-4}$  cm<sup>2</sup> V<sup>-1</sup> s<sup>-1</sup> than those of both PM6:Qx-PhF and PM6:Qx-PhCl ( $\mu_h = 5.08 \times 10^{-4}$  and  $4.62 \times 10^{-4}$  cm<sup>2</sup> V<sup>-1</sup> s<sup>-1</sup>;  $\mu_e = 2.18 \times 10^{-4}$  and  $1.31 \times 10^{-4}$  cm<sup>2</sup> V<sup>-1</sup> s<sup>-1</sup>, respectively). Importantly, PM6:Qx-PhBr has a more balanced charge carrier mobility ratio ( $\mu_e/\mu_h = 0.63$ ) than those of PM6:Qx-PhF and PM6:Qx-PhCl ( $\mu_e/\mu_h = 0.43$  and 0.28, respectively) blends. The enhanced and more balanced electron/hole mobility in the PM6:Qx-PhBr blend contributes to more favorable charge extraction and charge transport, and thus, higher FF and PCE are obtained. Next, to gain a deeper understanding of the charge recombination and

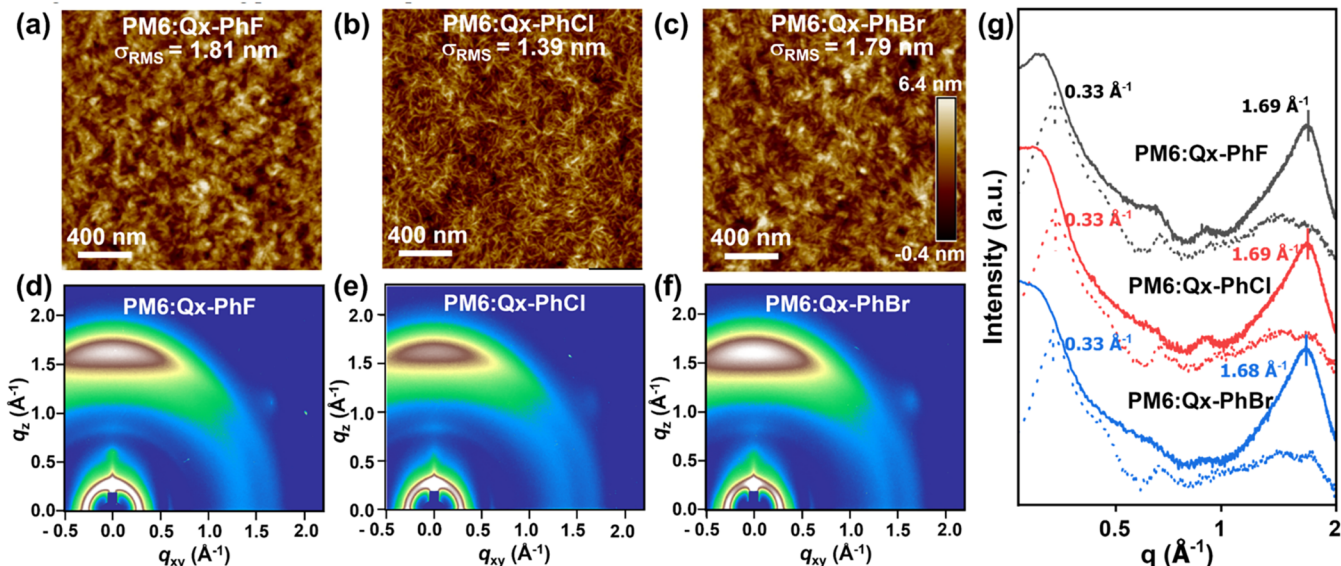


**Figure 4.** (a–c). AFM height images, (d–f) 2D GIWAXS patterns of the indicated blend films, and (g) corresponding line-cut profiles of the indicated blend films.

extraction behaviors, transient photocurrent (TPC) and transient photovoltage (TPV) evaluations were conducted.<sup>76</sup> The charge extraction time and carrier lifetime were extracted from the TPC and TPV decay dynamics through mono-exponential fits. As shown in Figure 3h, the PM6:Qx-PhBr OSCs exhibit a slightly shorter charge extraction time of 0.20  $\mu$ s than those of the PM6:Qx-PhF (0.27  $\mu$ s) and PM6:Qx-PhCl (0.31  $\mu$ s) blends, indicating that the PM6:Qx-PhBr-based OSCs extract charge carriers more rapidly. Furthermore, the carrier lifetimes ( $\tau$ ) derived from the TPV measurements (Figure 3i) are significantly longer for the PM6:Qx-PhBr blend at 6.52  $\mu$ s versus 1.82 and 1.30  $\mu$ s for PM6:Qx-PhF and PM6:Qx-PhCl-based devices, respectively, consistent with reduced charge recombination in the PM6:Qx-PhBr devices. Consequently, more efficient charge extraction and reduced free charge recombination explain the higher  $J_{SC}$  and FF values (see details in Table 2) observed in the PM6:Qx-PhBr OSCs.

#### Thin-Film Morphology and Microstructure Analysis

To gain a comprehensive understanding of the morphology, atomic force microscopy (AFM) and transmission electron microscopy (TEM) were applied to elucidate phase separation in the active layer. AFM imaging (Figures 4 and S12) reveals that the PM6:Qx-PhF, PM6:Qx-PhCl, and PM6:Qx-PhBr blends exhibit a uniform surface morphology with root-mean-square (RMS) roughnesses of 1.81, 1.39, and 1.79 nm, respectively. However, compared with the PM6:Qx-PhF film, the PM6:Qx-PhCl and PM6:Qx-PhBr blends possess relatively pronounced nanofibril morphologies. Interestingly, the brominated PM6:Qx-PhBr thin film exhibits a larger diameter fiber structure in comparison with that of PM6:Qx-PhCl (~27 vs. ~22 nm), resulting in a favorable phase-separated morphology (Figures S12–S13).<sup>77,78</sup> These results indicate that the PM6:Qx-PhBr blend has an ideal morphology that is beneficial for exciton dissociation and charge transport, in conformity with the aforementioned reduced recombination loss and enhanced charge mobility.

Grazing-incidence wide-angle X-ray scattering (GIWAXS) was next employed to investigate the molecular packing and crystallinity of the neat NFAs and their corresponding blend

films. The GIWAXS patterns and the corresponding line cuts for the blend films are provided in Figures 4d–g and S14–S15, and all data are summarized in Tables S6–S9. As shown in Figure S14, the neat NFAs exhibit a preferential  $\pi$ -face-on orientation of the conjugated backbone with respect to the substrate surface, as evidenced by the strong  $\pi-\pi$  (010) stacking peak at around  $q_x = 1.64\text{--}1.69 \text{ \AA}^{-1}$  in the out-of-plane (OOP) direction and a diffraction peak of (100) at around  $q_{xy} = 0.37\text{--}0.38 \text{ \AA}^{-1}$  in the in-plane (IP) direction. From the in-plane (100) reflection ( $q_{xy}$ ), it is found that when the halogen atomic number increases from F to Br, the lamellar  $d$ -spacing ( $d_l$ ) contracts from 17.1  $\text{\AA}$  (Qx-PhF), to 16.4  $\text{\AA}$  (Qx-PhCl) and 16.4  $\text{\AA}$  (Qx-PhBr), and the crystal coherence length (CCL) falls from 72.4 to 33.6 to 42.0  $\text{\AA}$ . For the (010) out-of-plane reflections, the  $\pi-\pi$  intermolecular  $d$ -spacing distance ( $d_\pi$ ) is similar within the range from 3.7 to 3.8  $\text{\AA}$ . The GIWAXS data for the blend films indicate similar preferential face-on  $\pi-\pi$  intermolecular stacking distributions of the donor polymer chains with respect to the substrate surface (Figure 4), as evidenced by the strong  $\pi-\pi$  (010) stacking peak at around  $q_x = 1.68\text{--}1.69 \text{ \AA}^{-1}$  in the OOP direction and a diffraction peak of (100) at around  $q_{xy} \approx 0.33 \text{ \AA}^{-1}$  in the IP direction. For the PM6:Qx-PhF, PM6:Qx-PhCl, and PM6:Qx-PhBr blends, the reflections located at  $q_{xy} \approx 0.33 \text{ \AA}^{-1}$  are attributed to the donor polymer (100) alkyl-chain stacking. Upon increasing the halogen atomic radius in the blend (F  $\rightarrow$  Br), the  $d_l$  remains constant at  $\sim$ 19  $\text{\AA}$ , while the CCL monotonically increases from 95.3  $\text{\AA}$  (PM6:Qx-PhF), 95.8  $\text{\AA}$  (PM6:Qx-PhCl) to 106.1  $\text{\AA}$  (PM6:Qx-PhBr). For the out-of-plane direction, almost identical  $\pi-\pi$  stacking (010) diffraction peaks are found at  $q_z = 1.68\text{--}1.69 \text{ \AA}^{-1}$ . The calculated  $d_\pi$  values are 3.72, 3.72, and 3.75  $\text{\AA}$ , and the corresponding CCL values are 22.7  $\text{\AA}$  for PM6:Qx-PhF, 22.7  $\text{\AA}$  for PM6:Qx-PhCl, and 21.6  $\text{\AA}$  for PM6:Qx-PhBr blend. However, the  $\pi$ -stacking intensity gradually increases from PM6:Qx-PhF to PM6:Qx-PhBr, suggesting a greater order.

Additionally, in order to qualitatively assess the D–A miscibility, the water and formamide contact angles of donors and acceptors were measured to calculate the surface tension ( $\gamma$ ) and Flory–Huggins interaction parameter ( $\chi_{\text{donor-acceptor}}$ )

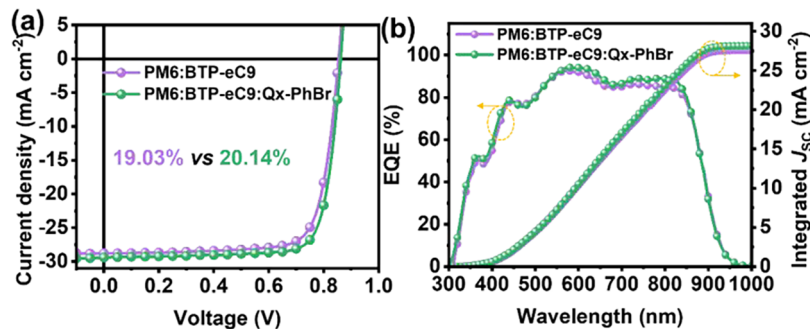


**Figure 5.** (a)  $J$ – $V$  and (b) EQE curves of the indicated binary and ternary devices.

(Figure S16 and Table S8). The aqueous contact angles of **PM6**, **Qx-PhF**, **Qx-PhCl**, and **Qx-PhBr** films are  $106.82^\circ$ ,  $102.10^\circ$ ,  $96.65^\circ$ , and  $96.36^\circ$ , respectively, while the formamide contact angles are  $84.33$ ,  $74.78$ ,  $74.74$ , and  $74.44^\circ$ , respectively, resulting in  $\gamma$  for **PM6**, **Qx-PhF**, **Qx-PhCl**, and **Qx-PhBr** films of  $22.56$ ,  $31.38$ ,  $26.48$ , and  $26.64$  mN m<sup>-1</sup>, respectively. Therefore, the calculated  $\chi$  value of the blends with **PM6** are  $0.73$ ,  $0.16$ , and  $0.16$  for **PM6:Qx-PhF**, **PM6:Qx-PhCl**, and **PM6:Qx-PhBr**, respectively, implying a far greater miscibility of **Qx-PhCl** and **Qx-PhBr** with **PM6**. These results demonstrate that the halogenation of the central unit of **Qx-PhHal** NFAs greatly affects the D–A miscibility, affording a heretofore unrecognized opportunity to manipulate OSC morphologies favoring a nanofibril morphology that enhances optoelectronic properties.<sup>79,80</sup>

Finally, the ESP of **PM6** and new synthesized NFAs **Qx-PhF**, **Qx-PhCl**, and **Qx-PhBr** were computed to probe how the intermolecular interaction affects the charge generation and recombination (Figure S3). Although the molecular conformation minimally changes upon different NFA halogenations, the difference in ESP between **Qx-PhBr** and **PM6** monomer is larger than that of **Qx-PhF** or **Qx-PhCl** and **PM6**. It is well-recognized that larger differences in ESP between the donor and acceptor lead to stronger intermolecular interactions,<sup>81</sup> which aligns with the present superior miscibility of **Qx-PhBr** and **PM6** and the aforementioned photovoltaic findings.

Molecular dynamics simulations of **PM6:Qx-PhF**, **PM6:Qx-PhCl**, and **PM6:Qx-PhBr** blends were carried out (Figure S17). In the **PM6:Qx-PhBr** blend, the first peaks of the D–D g(r) curves appear at a greatly shorter distance compared to those in the **PM6:Qx-PhF** and **PM6:Qx-PhCl** blends. This data corroborate enhanced molecular packing as well as stronger intermolecular interactions within the donor and acceptor domains in the former blend, respectively, which is the key characteristic for promoting more ordered structures with enhanced charge transport. Additionally, the first A–A and D–A g(r) peak in **PM6:Qx-PhCl** and **PM6:Qx-PhBr** is located at a shorter distance than that in **PM6:Qx-PhF**, implying stronger acceptor–acceptor and donor–acceptor interactions in the former blends. These results are aligned with the morphology characterizations.

### Ternary Solar Cells

The ternary formulation of mixing acceptors is a common strategy to further improve OSC performance.<sup>53,82</sup> As a high-efficiency binary OSC system, **PM6:BTP-eC9** has garnered considerable attention. Therefore, we introduced brominated NFA **Qx-PhBr** into **PM6:BTP-eC9** as the third component to

demonstrate that further PCE enhancement is possible (Figure S18). The optimal  $J$ – $V$  curves for the binary and ternary systems are shown in Figure 5, and the device parameters are summarized in Table S11. The control binary device based on **PM6:BTP-eC9** exhibits a PCE of  $19.03\%$  with a  $V_{OC} = 0.85$  V,  $J_{SC} = 28.78$  mA cm<sup>-2</sup>, and FF =  $77.38\%$ , which is consistent with the literature values.<sup>83</sup> Upon incorporation of **Qx-PhBr** into the **PM6:BTP-eC9** blend, the resulting ternary device exhibits an elevated  $V_{OC}$  of  $0.86$  V,  $J_{SC}$  of  $29.40$  mA cm<sup>-2</sup>, and FF of  $79.50\%$ , thus delivering a remarkable PCE of  $20.14\%$ . All devices exhibit broad photoresponse ranging from  $300$  to  $900$  nm (Figures 5 and S19). Compared to the binary OSCs, the ternary OSCs with **Qx-PhBr** exhibit relatively higher photoresponse, which contributes to the enhanced  $J_{SC}$  values. Moreover, the  $J_{SC}$  values calculated from the integration of the EQE spectra are  $27.57$  and  $28.14$  mA cm<sup>-2</sup>, respectively, in alignment with the corresponding  $J$ – $V$  curves (within 5% mismatch). Additionally, the thermal stability of these OSCs was recorded at  $80$  °C, and the corresponding binary and ternary OSCs exhibit identical PCE loss under this thermal stress condition (Figure S17). Additionally, despite the larger PCEs, the incorporation of **Qx-PhBr** into the **PM6:BTP-eC9** blend slightly improves the storage stability and light stability (Figure S21). These results highlight the suitability of a brominated NFA for enhancing the ternary photovoltaic performance.

### CONCLUSIONS

A series of **Qx-PhHal** NFAs systematically functionalized with the halogen atoms F, Cl, and Br central cores were characterized to understand how halogen substitution affects the electrostatic interactions, film microstructures, and OSC performance. Interestingly, the bromine-containing **PM6:Qx-PhBr** devices exhibit a higher PCE than those of the **PM6:Qx-PhF** and **PM6:Qx-PhCl** OSCs ( $17.58$  vs  $14.77\%$  and  $13.59\%$ ), which correlates with the enhanced  $V_{OC}$  ( $0.91$  vs  $0.88$  and  $0.89$  V),  $J_{SC}$  ( $25.59$  vs  $22.56$  and  $21.49$  mA cm<sup>-2</sup>), and FF ( $75.53$  vs  $74.22\%$  and  $71.21\%$ ). DFT computations reveal that bromination promotes blend electrostatic interactions, and film morphological analysis indicates that **PM6:Qx-PhBr** blends exhibit a pronounced nanofibril morphology. Detailed analysis of exciton dissociation, carrier recombination, D–A miscibility, and charge transport reveals that **PM6:Qx-PhBr** exhibits a larger and more balanced  $\mu_e/\mu_h$ , more efficient exciton dissociation, enhanced charge collection capacity, and reduced bimolecular recombination compared to the analogous **PM6:Qx-PhF** and **PM6:Qx-PhCl** blends. Finally, ternary solar cells employing **Qx-PhBr** as the third component realize a PCE of  $20.14\%$ . This study began with theoretical

computation to systematically investigate the impact of various halogen substitutions at the central core, leading to the development of high-performance OSCs. These results highlight the vital role and versatility of fine-tuning acceptor structures, particularly through the incorporation of heavier halogens.

## ■ ASSOCIATED CONTENT

### SI Supporting Information

The Supporting Information is available free of charge at <https://pubs.acs.org/doi/10.1021/jacs.5c16058>.

Experimental section, materials synthesis, NMR spectra and mass spectra, cyclic voltammetry, thermogravimetric analysis, DFT calculation, grazing-incidence wide-angle X-ray scattering, solar cell device stability, space-charge-limited current measurement, effective voltage and light intensity measurements, contact angle measurement, miscibility analyses, and references ([PDF](#))

## ■ AUTHOR INFORMATION

### Corresponding Authors

**Yao Chen** — Chongqing Institute of Green and Intelligent Technology, Chinese Academy of Sciences, Chongqing 400714, P. R. China; Chongqing School, University of Chinese Academy of Sciences, Chongqing 400714, P. R. China;  [orcid.org/0000-0003-4414-8528](https://orcid.org/0000-0003-4414-8528);  
Email: [chenyao@cigit.ac.cn](mailto:chenyao@cigit.ac.cn)

**Zeyun Xiao** — Chongqing Institute of Green and Intelligent Technology, Chinese Academy of Sciences, Chongqing 400714, P. R. China; Chongqing School, University of Chinese Academy of Sciences, Chongqing 400714, P. R. China;  [orcid.org/0000-0002-5082-5663](https://orcid.org/0000-0002-5082-5663);  
Email: [xiao.z@cigit.ac.cn](mailto:xiao.z@cigit.ac.cn)

**Tobin J. Marks** — Department of Chemistry, the Materials Research Center, Trienens Institute for Sustainability and Energy, Northwestern University, Evanston, Illinois 60208, United States;  [orcid.org/0000-0001-8771-0141](https://orcid.org/0000-0001-8771-0141);  
Email: [t-marks@northwestern.edu](mailto:t-marks@northwestern.edu)

**Antonio Facchetti** — Department of Chemistry, the Materials Research Center, Trienens Institute for Sustainability and Energy, Northwestern University, Evanston, Illinois 60208, United States; School of Materials Science and Engineering, Georgia Institute of Technology, Atlanta, Georgia 30332, United States;  [orcid.org/0000-0002-8175-7958](https://orcid.org/0000-0002-8175-7958);  
Email: [antonio.facchetti@mse.gatech.edu](mailto:antonio.facchetti@mse.gatech.edu)

### Authors

**Hongliang Lei** — Chongqing Institute of Green and Intelligent Technology, Chinese Academy of Sciences, Chongqing 400714, P. R. China; Chongqing School, University of Chinese Academy of Sciences, Chongqing 400714, P. R. China

**Seunglok Lee** — School of Energy and Chemical Engineering, Ulsan National Institute of Science and Technology (UNIST), Ulsan 44919, South Korea;  [orcid.org/0009-0006-1012-8202](https://orcid.org/0009-0006-1012-8202)

**Peihao Huang** — Chongqing Institute of Green and Intelligent Technology, Chinese Academy of Sciences, Chongqing 400714, P. R. China; Chongqing School, University of Chinese Academy of Sciences, Chongqing 400714, P. R. China

**Gengsui Tian** — Chongqing Institute of Green and Intelligent Technology, Chinese Academy of Sciences, Chongqing 400714, P. R. China; Chongqing School, University of Chinese Academy of Sciences, Chongqing 400714, P. R. China

**Lei Liu** — Chongqing Institute of Green and Intelligent Technology, Chinese Academy of Sciences, Chongqing 400714, P. R. China; Chongqing School, University of Chinese Academy of Sciences, Chongqing 400714, P. R. China

**Tianyu Zeng** — Chongqing Institute of Green and Intelligent Technology, Chinese Academy of Sciences, Chongqing 400714, P. R. China; Chongqing School, University of Chinese Academy of Sciences, Chongqing 400714, P. R. China

**Changduk Yang** — School of Energy and Chemical Engineering, Ulsan National Institute of Science and Technology (UNIST), Ulsan 44919, South Korea;  [orcid.org/0000-0001-7452-4681](https://orcid.org/0000-0001-7452-4681)

**Tainan Duan** — Chongqing Institute of Green and Intelligent Technology, Chinese Academy of Sciences, Chongqing 400714, P. R. China; Chongqing School, University of Chinese Academy of Sciences, Chongqing 400714, P. R. China;  [orcid.org/0000-0002-6010-4501](https://orcid.org/0000-0002-6010-4501)

**Huanyu Zhou** — School of Materials Science and Engineering, Georgia Institute of Technology, Atlanta, Georgia 30332, United States

Complete contact information is available at:  
<https://pubs.acs.org/10.1021/jacs.5c16058>

### Author Contributions

#Y.C. and H.L. contributed equally to this work.

### Notes

The authors declare no competing financial interest.

## ■ ACKNOWLEDGMENTS

Y.C. and H.L. contributed equally to this work. This work was financially supported by the National Natural Science Foundation of China (Nos. 22209169 and 22475211) and the Natural Science Foundation of Chongqing (CSTB2024NSCQ-Q\_C\_X\_M\_X\_0\_0\_9\_7 and CSTB2023NSCQMSX0611). T.J.M. and A.F. acknowledge support of this research by U.S. Office of Naval Research N00014-24-1-2109 (Northwestern U.) and N00014-24-1-2110 (Georgia Tech) and by the Northwestern University Materials Research Science and Engineering Center, NSF Award DMR-2308691.

## ■ REFERENCES

- (1) Zhang, X.; Qin, L.; Yu, J.; Li, Y.; Wei, Y.; Liu, X.; Lu, X.; Gao, F.; Huang, H. High-Performance Noncovalently Fused-Ring Electron Acceptors for Organic Solar Cells Enabled by Noncovalent Intramolecular Interactions and End-Group Engineering. *Angew. Chem., Int. Ed.* **2021**, *60* (22), 12475–12481.
- (2) Riede, M.; Spoltore, D.; Leo, K. Organic Solar Cells—The Path to Commercial Success. *Adv. Energy Mater.* **2021**, *11* (1), No. 2002653.
- (3) Cho, Y.; Sun, Z.; Li, G.; Zhang, D.; Yang, S.; Marks, T. J.; Yang, C.; Facchetti, A. CF(3)-Functionalized Side Chains in Nonfullerene Acceptors Promote Electrostatic Interactions for Highly Efficient Organic Solar Cells. *J. Am. Chem. Soc.* **2025**, *147* (1), 758–769.
- (4) Li, G.; Qin, F.; Jacobberger, R. M.; Mukherjee, S.; Jones, L. O.; Young, R. M.; Pankow, R. M.; Kerwin, B. P.; Flagg, L. Q.; Zheng, D.;

- Feng, L.-W.; Kohlstedt, K. L.; Sangwan, V. K.; Hersam, M. C.; Schatz, G. C.; DeLongchamp, D. M.; Wasielewski, M. R.; Zhou, Y.; Facchetti, A.; Marks, T. J. What is the role of non-fullerene acceptor symmetry in polymer solar cell efficiency? *Joule* **2023**, *7* (9), 2152–2173.
- (5) Zhang, J.; Tan, H. S.; Guo, X.; Facchetti, A.; Yan, H. Material insights and challenges for non-fullerene organic solar cells based on small molecular acceptors. *Nat. Energy* **2018**, *3* (9), 720–731.
- (6) Liao, C.-Y.; Chen, Y.; Lee, C.-C.; Wang, G.; Teng, N.-W.; Lee, C.-H.; Li, W.-L.; Chen, Y.-K.; Li, C.-H.; Ho, H.-L.; et al. Processing Strategies for an Organic Photovoltaic Module with over 10% Efficiency. *Joule* **2020**, *4* (1), 189–206.
- (7) Lin, Y.; Adilbekova, B.; Firdaus, Y.; Yengel, E.; Faber, H.; Sajjad, M.; Zheng, X.; Yarali, E.; Seitkhan, A.; Bakr, O. M.; et al. 17% Efficient organic solar cells based on liquid exfoliated WS<sub>2</sub> as a replacement for PEDOT: PSS. *Adv. Mater.* **2019**, *31* (46), No. 1902965.
- (8) Xie, Y.; Yang, F.; Li, Y.; Uddin, M. A.; Bi, P.; Fan, B.; Cai, Y.; Hao, X.; Woo, H. Y.; Li, W.; Liu, F.; Sun, Y. Morphology Control Enables Efficient Ternary Organic Solar Cells. *Adv. Mater.* **2018**, *30* (38), No. e1803045.
- (9) Wei, Y. A.; Yu, J. W.; Qin, L. Q.; Chen, H.; Wu, X. X.; Wei, Z. X.; Zhang, X.; Xiao, Z.; Ding, L. M.; Gao, F.; Huang, H. A universal method for constructing high efficiency organic solar cells with stacked structures. *Energy Environ. Sci.* **2021**, *14* (4), 2314–2321.
- (10) Liao, C.; Xu, X.; Yang, T.; Qiu, W.; Duan, Y.; Li, R.; Yu, L.; Peng, Q. Tetrahydrofuran Processable Organic Solar Cells with 19.45% Efficiency Realized by Introducing High Molecular Dipole Unit Into the Terpolymer. *Adv. Mater.* **2024**, *36* (48), No. e2411071.
- (11) Deng, M.; Xu, X.; Qiu, W.; Duan, Y.; Li, R.; Yu, L.; Peng, Q. Improving Miscibility of Polymer Donor and Polymer Acceptor by Reducing Chain Entanglement for Realizing 18.64% Efficiency All Polymer Solar Cells. *Angew. Chem., Int. Ed.* **2024**, *63* (35), No. e202405243.
- (12) Zhu, W.; Li, G.; Mukherjee, S.; Powers-Riggs, N. E.; Jones, L. O.; Gann, E.; Kline, R. J.; Herzing, A.; Logsdon, J. L.; Flagg, L.; Stern, C. L.; Young, R. M.; Kohlstedt, K. L.; Schatz, G. C.; DeLongchamp, D. M.; Wasielewski, M. R.; Melkonyan, F. S.; Facchetti, A.; Marks, T. J. Quantitative relationships between film morphology, charge carrier dynamics, and photovoltaic performance in bulk-heterojunction binary vs. ternary acceptor blends. *Energy Environ. Sci.* **2023**, *16* (3), 1234–1250.
- (13) Zhu, L.; Zhang, M.; Zhou, G.; Wang, Z.; Zhong, W.; Zhuang, J.; Zhou, Z.; Gao, X.; Kan, L.; Hao, B.; Han, F.; Zeng, R.; Xue, X.; Xu, S.; Jing, H.; Xiao, B.; Zhu, H.; Zhang, Y.; Liu, F. Achieving 20.8% organic solar cells via additive-assisted layer-by-layer fabrication with bulk p-i-n structure and improved optical management. *Joule* **2024**, *8* (11), 3153–3168.
- (14) Wang, S.; Wang, S.; Wang, J.; Yu, N.; Qiao, J.; Xie, X.; Li, C.; Abbasi, M. S.; Ding, R.; Zhang, X.; Han, Y.; Lu, G.; Zhang, J.; Hao, X.; Tang, Z.; Cai, Y.; Huang, H. Achieving 20% Efficiency in Organic Solar Cells Through Conformationally Locked Solid Additives. *Adv. Energy Mater.* **2025**, No. 2405205.
- (15) Gu, X.; Wei, Y.; Zeng, R.; Lv, J.; Hou, Y.; Yu, N.; Tan, S.; Wang, Z.; Li, C.; Tang, Z.; Peng, Q.; Liu, F.; Cai, Y.; Zhang, X.; Huang, H. Suppressing Exciton-Vibration Coupling via Intramolecular Noncovalent Interactions for Low-Energy-Loss Organic Solar Cells. *Angew. Chem., Int. Ed.* **2025**, *64* (7), No. e202418926.
- (16) Wu, J.; Fu, C.; Chen, B.; Rong, X.; Lu, Z.; Huang, Y. Isomeric Effect of a pi Bridge in an IDT-Based Nonfused Electron Photovoltaic Acceptor. *Chem. - Eur. J.* **2024**, *30* (1), No. e202302624.
- (17) Pang, Z. G.; Zhang, W. F.; Wu, J. L.; Luo, Y. J.; Liu, J. S.; Zhao, S. L.; Xu, Z.; Lu, Z. Y.; Huang, Y. Insight into the effects of alkoxy side chain position in nonfullerene electron acceptors on the morphological stability of organic solar cells. *Dyes Pig.* **2020**, *181*, No. 108562.
- (18) Wu, J.; Chen, Y.; Hu, B.; Pang, Z.; Lu, Z.; Huang, Y. Isomers of Dithienocyclopentapyrene-Based Non-Fullerene Electron Acceptors: Configuration Effect on Photoelectronic Properties. *Chem. - Eur. J.* **2019**, *25* (25), 6385–6391.
- (19) Li, C.; Song, J.; Lai, H.; Zhang, H.; Zhou, R.; Xu, J.; Huang, H.; Liu, L.; Gao, J.; Li, Y.; Jee, M. H.; Zheng, Z.; Liu, S.; Yan, J.; Chen, X. K.; Tang, Z.; Zhang, C.; Woo, H. Y.; He, F.; Gao, F.; Yan, H.; Sun, Y. Non-fullerene acceptors with high crystallinity and photoluminescence quantum yield enable > 20% efficiency organic solar cells. *Nat. Mater.* **2025**, *24* (3), 433–443.
- (20) He, H.; Li, X.; Zhang, J.; Chen, Z.; Gong, Y.; Zhuo, H.; Wu, X.; Li, Y.; Wang, S.; Bi, Z.; Song, B.; Zhou, K.; Liang, T.; Ma, W.; Lu, G.; Ye, L.; Meng, L.; Zhang, B.; Li, Y.; Li, Y. Dynamic hydrogen-bonding enables high-performance and mechanically robust organic solar cells processed with non-halogenated solvent. *Nat. Commun.* **2025**, *16* (1), No. 787.
- (21) Li, G.; Feng, L.-W.; Mukherjee, S.; Jones, L. O.; Jacobberger, R. M.; Huang, W.; Young, R. M.; Pankow, R. M.; Zhu, W.; Lu, N.; Kohlstedt, K. L.; Sangwan, V. K.; Wasielewski, M. R.; Hersam, M. C.; Schatz, G. C.; DeLongchamp, D. M.; Facchetti, A.; Marks, T. J. Non-fullerene acceptors with direct and indirect hexa-fluorination afford > 17% efficiency in polymer solar cells. *Energy Environ. Sci.* **2022**, *15* (2), 645–659.
- (22) Karki, A.; Gillett, A. J.; Friend, R. H.; Nguyen, T. Q. The Path to 20% Power Conversion Efficiencies in Nonfullerene Acceptor Organic Solar Cells. *Adv. Energy Mater.* **2020**, *11* (15), No. 2003441.
- (23) Lin, Y.; Wang, J.; Zhang, Z. G.; Bai, H.; Li, Y.; Zhu, D.; Zhan, X. An electron acceptor challenging fullerenes for efficient polymer solar cells. *Adv. Mater.* **2015**, *27* (7), 1170–1174.
- (24) Zhao, W.; Qian, D.; Zhang, S.; Li, S.; Inganas, O.; Gao, F.; Hou, J. Fullerene-Free Polymer Solar Cells with over 11% Efficiency and Excellent Thermal Stability. *Adv. Mater.* **2016**, *28* (23), 4734–4739.
- (25) Zhao, W.; Li, S.; Yao, H.; Zhang, S.; Zhang, Y.; Yang, B.; Hou, J. Molecular Optimization Enables over 13% Efficiency in Organic Solar Cells. *J. Am. Chem. Soc.* **2017**, *139* (21), 7148–7151.
- (26) Li, W.; Ye, L.; Li, S.; Yao, H.; Ade, H.; Hou, J. A High-Efficiency Organic Solar Cell Enabled by the Strong Intramolecular Electron Push-Pull Effect of the Nonfullerene Acceptor. *Adv. Mater.* **2018**, *30* (16), No. 1707170.
- (27) Zhu, L.; Zhang, M.; Xu, J.; Li, C.; Yan, J.; Zhou, G.; Zhong, W.; Hao, T.; Song, J.; Xue, X.; Zhou, Z.; Zeng, R.; Zhu, H.; Chen, C. C.; MacKenzie, R. C. I.; Zou, Y.; Nelson, J.; Zhang, Y.; Sun, Y.; Liu, F. Single-junction organic solar cells with over 19% efficiency enabled by a refined double-fibril network morphology. *Nat. Mater.* **2022**, *21* (6), 656–663.
- (28) Wu, J.; Liao, C. Y.; Chen, Y.; Jacobberger, R. M.; Huang, W.; Zheng, D.; Tsai, K. W.; Li, W. L.; Lu, Z.; Huang, Y.; Wasielewski, M. R.; Chang, Y. M.; Marks, T. J.; Facchetti, A. To Fluorinate or Not to Fluorinate in Organic Solar Cells: Achieving a Higher PCE of 15.2% when the Donor Polymer is Halogen-Free. *Adv. Energy Mater.* **2021**, *11* (47), No. e2102648.
- (29) Swick, S. M.; Zhu, W.; Matta, M.; Aldrich, T. J.; Harbzaru, A.; Lopez Navarrete, J. T.; Ponce Ortiz, R.; Kohlstedt, K. L.; Schatz, G. C.; Facchetti, A.; Melkonyan, F. S.; Marks, T. J. Closely packed, low reorganization energy pi-extended postfullerene acceptors for efficient polymer solar cells. *Proc. Natl. Acad. Sci. USA* **2018**, *115* (36), E8341–E8348.
- (30) Zhang, X.; Li, G.; Mukherjee, S.; Huang, W.; Zheng, D.; Feng, L. W.; Chen, Y.; Wu, J.; Sangwan, V. K.; Hersam, M. C.; DeLongchamp, D. M.; Yu, J.; Facchetti, A.; Marks, T. J. Systematically Controlling Acceptor Fluorination Optimizes Hierarchical Morphology, Vertical Phase Separation, and Efficiency in Non-Fullerene Organic Solar Cells. *Adv. Energy Mater.* **2021**, *12* (1), No. 2102172.
- (31) Zou, B.; Liang, A.; Ding, P.; Yao, J.; Zeng, X.; Li, H.; Ma, R.; Li, C.; Wu, W.; Chen, D.; Qamar, M.; Yu, H.; Yi, J.; Guo, L.; Pun, S. H.; Halpert, J. E.; Li, G.; Kan, Z.; Yan, H. Dipole Moment Modulation of Terminal Groups Enables Asymmetric Acceptors Featuring Medium Bandgap for Efficient and Stable Ternary Organic Solar Cells. *Angew. Chem., Int. Ed.* **2025**, *64* (3), No. e202415332.
- (32) Zhou, W.; Liu, J.; Xie, J.; You, S.; Deng, J.; Yu, F.; Jeong, S. Y.; Woo, H. Y.; Wu, F.; Chen, L. Non-Fused Star-Shape Giant Trimer

- Electron Acceptors for Organic Solar Cells with Efficiency over 19%. *Angew. Chem., Int. Ed.* **2025**, *64* (3), No. e202415141.
- (33) Yuan, J.; Zhang, Y.; Zhou, L.; Zhang, G.; Yip, H.-L.; Lau, T.-K.; Lu, X.; Zhu, C.; Peng, H.; Johnson, P. A.; Leclerc, M.; Cao, Y.; Ulanski, J.; Li, Y.; Zou, Y. Single-Junction Organic Solar Cell with over 15% Efficiency Using Fused-Ring Acceptor with Electron-Deficient Core. *Joule* **2019**, *3* (4), 1140–1151.
- (34) Zhu, W.; Spencer, A. P.; Mukherjee, S.; Alzola, J. M.; Sangwan, V. K.; Amsterdam, S. H.; Swick, S. M.; Jones, L. O.; Heiber, M. C.; Herzing, A. A.; Li, G.; Stern, C. L.; DeLongchamp, D. M.; Kohlstedt, K. L.; Hersam, M. C.; Schatz, G. C.; Wasielewski, M. R.; Chen, L. X.; Facchetti, A.; Marks, T. J. Crystallography, Morphology, Electronic Structure, and Transport in Non-Fullerene/Non-Indacenodithienothiophene Polymer:Y6 Solar Cells. *J. Am. Chem. Soc.* **2020**, *142* (34), 14532–14547.
- (35) Wu, X.; Gong, Y.; Li, X.; Qin, S.; He, H.; Chen, Z.; Liang, T.; Wang, C.; Deng, D.; Bi, Z.; Ma, W.; Meng, L.; Li, Y. Inner Side Chain Modification of Small Molecule Acceptors Enables Lower Energy Loss and High Efficiency of Organic Solar Cells Processed with Non-halogenated Solvents. *Angew. Chem., Int. Ed.* **2025**, *64* (4), No. e202416016.
- (36) Zhou, X. L.; Liang, W. T.; Ma, R. J.; Zhang, C. F.; Peng, Z. X.; Dela Pena, T. A.; Wu, J. Y.; Ma, Z. F.; Liao, Y. Z.; Li, G.; Hu, H. W. Synergistic control of multilength-scale morphology and vertical phase separation for high-efficiency organic solar cells. *Energy Environ. Sci.* **2024**, *17* (20), 7762–7771.
- (37) Zhang, R.; Chen, H. Y.; Wang, T. H.; Kobera, L.; He, L. L.; Huang, Y. T.; Ding, J. Y.; Zhang, B.; Khasbaatar, A.; Nanayakkara, S.; Zheng, J. L.; Chen, W. J.; Diao, Y.; Abbret, S.; Brus, J.; Coffey, A. H.; Zhu, C. H.; Liu, H.; Lu, X. H.; Jiang, Q.; Coropceanu, V.; Brédas, J. L.; Li, Y. F.; Li, Y. W.; Gao, F. Equally high efficiencies of organic solar cells processed from different solvents reveal key factors for morphology control. *Nat. Energy* **2025**, *10* (1), 124–134.
- (38) Gu, X.; Zeng, R.; Hou, Y.; Yu, N.; Qiao, J.; Li, H.; Wei, Y.; He, T.; Zhu, J.; Deng, J.; Tan, S.; Zhang, C.; Cai, Y.; Long, G.; Hao, X.; Tang, Z.; Liu, F.; Zhang, X.; Huang, H. Precisely Regulating Intermolecular Interactions and Molecular Packing of Nonfused-Ring Electron Acceptors via Halogen Transposition for High-Performance Organic Solar Cells. *Angew. Chem., Int. Ed.* **2024**, *63* (34), No. e202407355.
- (39) Yao, H. F.; Wang, J. W.; Xu, Y.; Hou, J. H. Terminal Groups of Nonfullerene Acceptors: Design and Applications. *Chem. Mater.* **2023**, *35* (3), 807–821.
- (40) Luo, Z.; Yan, H.; Yang, C. End-Group Engineering of Nonfullerene Acceptors for High-Efficiency Organic Solar Cells. *Acc. Mater. Res.* **2023**, *4* (11), 968–981.
- (41) Wang, H.; Liu, T.; Zhou, J. D.; Mo, D. Z.; Han, L.; Lai, H. J.; Chen, H.; Zheng, N.; Zhu, Y. L.; Xie, Z. Q.; He, F. Bromination: An Alternative Strategy for Non-Fullerene Small Molecule Acceptors. *Adv. Sci.* **2020**, *7* (9), No. 1903784.
- (42) Cui, Y.; Yao, H.; Zhang, J.; Xian, K.; Zhang, T.; Hong, L.; Wang, Y.; Xu, Y.; Ma, K.; An, C.; He, C.; Wei, Z.; Gao, F.; Hou, J. Single-Junction Organic Photovoltaic Cells with Approaching 18% Efficiency. *Adv. Mater.* **2020**, *32* (19), No. 1908205.
- (43) He, D.; Xie, L.; Bai, Y.; Zhang, H.; Liu, L.; Kong, J.; Chai, Y.; Li, X.; Wang, M.; Zhang, Y.; Zhang, J.; Li, Y.; Gao, F.; Guldi, D. M.; Zhao, F. Achieving High Fill Factor via Increasing Interfacial Disorder to Inhibit Bimolecular Recombination for Efficient Organic Solar Cells. *Angew. Chem., Int. Ed.* **2025**, *64* (25), No. e202505722.
- (44) Mou, H.; Yin, Y.; Chen, H.; Xu, J.; Ding, J.; Ju, C.; Zhu, J.; Wang, Y.; Chen, W.; Xu, G.; Zhang, T.; Li, J.; Li, Y.; Li, Y. Transient Dipole Strategy Boosts Highly Oriented Self-Assembled Monolayers for Organic Solar Cells Approaching 21% Efficiency. *J. Am. Chem. Soc.* **2025**, *147* (24), 21241–21251.
- (45) Liang, H.; Bi, X.; Chen, H.; He, T.; Lin, Y.; Zhang, Y.; Ma, K.; Feng, W.; Ma, Z.; Long, G.; Li, C.; Kan, B.; Zhang, H.; Rakitin, O. A.; Wan, X.; Yao, Z.; Chen, Y. A rare case of brominated small molecule acceptors for high-efficiency organic solar cells. *Nat. Commun.* **2023**, *14* (1), No. 4707.
- (46) Feng, J.; Yuan, Y.; Yang, H.; Tao, Y.; Hu, K. W.; Li, K.; Qian, J. H.; Hu, J. L.; Zhu, X. C.; Wu, Y.; Cui, C. H. Halogen Substituent Engineering in the Quinoxaline-based Central Unit of Acceptor for Efficient Organic Solar Cells. *Adv. Funct. Mater.* **2025**, No. e11955.
- (47) Qiu, D.; Zhang, J.; Lu, K.; Wei, Z. Halogenated thiophene substitutions on quinoxaline unit to achieve morphology optimization in efficient organic solar cells. *Nano Res.* **2023**, *16* (9), 11630–11637.
- (48) Xie, M.; Wei, Z.; Lu, K. Quinoxaline-based Y-type acceptors for organic solar cells. *Chem. Sci.* **2024**, *15* (22), 8265–8279.
- (49) Liu, K.; Jiang, Y.; Ran, G.; Liu, F.; Zhang, W.; Zhu, X. 19.7% efficiency binary organic solar cells achieved by selective core fluorination of nonfullerene electron acceptors. *Joule* **2024**, *8* (3), 835–851.
- (50) Liu, K. R.; Jiang, Y. Y.; Liu, F.; Zhu, X. Z. Quinoxaline-based nonfullerene acceptors with powerful core-functionalization ability enabling efficient solar energy utilization. *Energy Environ. Sci.* **2024**, *17* (14), 4944–4967.
- (51) Liu, H.; Geng, Y.; Xiao, Z.; Ding, L.; Du, J.; Tang, A.; Zhou, E. The Development of Quinoxaline-Based Electron Acceptors for High Performance Organic Solar Cells. *Adv. Mater.* **2024**, *36* (33), No. e2404660.
- (52) Wang, J.; Wang, P.; Chen, T.; Zhao, W.; Wang, J.; Lan, B.; Feng, W.; Liu, H.; Liu, Y.; Wan, X.; Long, G.; Kan, B.; Chen, Y. Isomerism Effect of 3D Dimeric Acceptors for Non-Halogenated Solvent-Processed Organic Solar Cells with 20% Efficiency. *Angew. Chem., Int. Ed.* **2024**, *64* (12), No. e202423562.
- (53) Chen, Z.; Ge, J.; Song, W.; Tong, X.; Liu, H.; Yu, X.; Li, J.; Shi, J.; Xie, L.; Han, C.; Liu, Q.; Ge, Z. 20.2% Efficiency Organic Photovoltaics Employing a pi-Extension Quinoxaline-Based Acceptor with Ordered Arrangement. *Adv. Mater.* **2024**, *36* (33), No. e2406690.
- (54) Xie, M.; Shi, Y.; Zhu, L.; Zhang, J.; Cheng, Q.; Zhang, H.; Yan, Y.; Zhu, M.; Zhou, H.; Lu, K.; Wei, Z. Selective halogenation of central and end-units of nonfullerene acceptors enables enhanced molecular packing and photovoltaic performance. *Energy Environ. Sci.* **2023**, *16* (8), 3543–3551.
- (55) Ran, X.; Zhang, C.; Qiu, D.; Tang, A.; Li, J.; Wang, T.; Zhang, J.; Wei, Z.; Lu, K. Cyanobenzene-Modified Quinoxaline-Based Acceptors with Optimal Excitonic Behavior Enable Efficient Organic Solar Cells. *Adv. Mater.* **2025**, *37* (32), No. e2504805.
- (56) Liu, K.; Jiang, Y.; Liu, F.; Ran, G.; Wang, M.; Wang, W.; Zhang, W.; Wei, Z.; Hou, J.; Zhu, X. The Critical Isomerization Effect of Core Bromination on Nonfullerene Acceptors in Achieving High-Performance Organic Solar Cells with Low Energy Loss. *Adv. Mater.* **2024**, *37* (7), No. e2413376.
- (57) Tao, J.; Yang, K.; Qiu, D.; Wang, C.; Zhang, H.; Lv, M.; Zhang, J.; Lu, K.; Wei, Z. Synergetic optimizing quinoxaline and selenophene substitution in non-fullerene acceptors for efficient organic solar cells. *Nano Energy* **2024**, *125*, No. 109540.
- (58) Lv, M.; Wang, Q. Y.; Zhang, J. Q.; Wang, Y. H.; Zhang, Z. G.; Wang, T.; Zhang, H.; Lu, K.; Wei, Z. X.; Deng, D. Strengthening the Hetero-Molecular Interactions in Giant Dimeric Acceptors Enables Efficient Organic Solar Cells. *Adv. Mater.* **2024**, *36* (4), No. e2310046.
- (59) Qiu, D.; Zhang, H.; Tian, C.; Zhang, J.; Zhu, L.; Wei, Z.; Lu, K. Central Core Substitutions and Film-formation Process Optimization Enable Approaching 19% Efficiency All-Polymer Solar Cells. *Adv. Mater.* **2023**, *35* (51), No. e2307398.
- (60) Yu, X. Q.; Zhu, J. T.; Xie, L.; Hu, H. T.; Liu, T. Q.; Ding, P. F.; Yu, X. L.; Ge, J. F.; Han, C. C.; Song, W.; Ge, Z. Y. Asymmetric nonfullerene acceptors with balanced crystallization kinetics enabling a trade-off between charge generation and recombination in ternary organic solar cells. *Energy Environ. Sci.* **2025**, *18* (12), 6094–6105.
- (61) Lai, S.; Cui, Y.; Chen, Z.; Xia, X.; Zhu, P.; Shan, S.; Hu, L.; Lu, X.; Zhu, H.; Liao, X.; Chen, Y. Impact of Electrostatic Interaction on Vertical Morphology and Energy Loss in Efficient Pseudo-Planar Heterojunction Organic Solar Cells. *Adv. Mater.* **2024**, *36* (18), No. e2313105.

- (62) Deng, M.; Tan, L.; Tang, H.; Peng, Q. Recent progress in Y-series small molecule acceptors in polymer solar cells. *Chem. Commun.* **2025**, *61* (53), 9569–9583.
- (63) Ma, S.; Li, H.; Wu, W.; Gamez-Valenzuela, S.; Ma, R.; Bai, Q.; Zhong, J.; Jeong, S. Y.; Liu, Q.; Zhang, H.; Zhang, G.; Zhang, W.; Chen, J.; Huang, E.; Liu, B.; Feng, K.; Woo, H. Y.; Niu, L.; Sun, H.; Guo, X. Chlorinated Bithiophene Imide-Based n-Type Polymers: Synthesis, Structure-Property Correlations, and Applications in Organic Electronic Devices. *Angew. Chem., Int. Ed.* **2025**, *64* (19), No. e202423616.
- (64) Wang, G.; Swick, S. M.; Matta, M.; Mukherjee, S.; Strzalka, J. W.; Logsdon, J. L.; Fabiano, S.; Huang, W.; Aldrich, T. J.; Yang, T.; Timalsina, A.; Powers-Riggs, N.; Alzola, J. M.; Young, R. M.; DeLongchamp, D. M.; Wasielewski, M. R.; Kohlstedt, K. L.; Schatz, G. C.; Melkonyan, F. S.; Facchetti, A.; Marks, T. J. Photovoltaic Blend Microstructure for High Efficiency Post-Fullerene Solar Cells. To Tilt or Not To Tilt? *J. Am. Chem. Soc.* **2019**, *141* (34), 13410–13420.
- (65) Schopp, N.; Brus, V. V.; Lee, J.; Dixon, A.; Karki, A.; Liu, T.; Peng, Z.; Graham, K. R.; Ade, H.; Bazan, G. C.; Nguyen, T. Q. Effect of Palladium-Tetrakis(Triphenylphosphine) Catalyst Traces on Charge Recombination and Extraction in Non-Fullerene-based Organic Solar Cells. *Adv. Funct. Mater.* **2021**, *31* (15), No. 2009363.
- (66) Xu, C.; Yang, J.; Gámez-Valenzuela, S.; Lee, J.-W.; Che, J.; Chen, P.; Zhang, G.; Hu, D.; Wang, Y.; Lv, J.; Zhong, Z.; Chen, X.; Zhang, G.; Zhao, F.; Kim, B. J.; Guo, X.; Liu, B. A bithiophene imide-based polymer donor for alloy-like ternary organic solar cells with over 20.5% efficiency and enhanced stability. *Energy Environ. Sci.* **2025**, *18* (12), 5913–5925.
- (67) Proctor, C. M.; Kim, C.; Neher, D.; Nguyen, T. Q. Nongeminate Recombination and Charge Transport Limitations in Diketopyrrolopyrrole-Based Solution-Processed Small Molecule Solar Cells. *Adv. Funct. Mater.* **2013**, *23* (28), 3584–3594.
- (68) Deng, M.; Xu, X.; Duan, Y.; Qiu, W.; Yu, L.; Li, R.; Peng, Q. 19.32% Efficiency Polymer Solar Cells Enabled by Fine-Tuning Stacking Modes of Y-Type Molecule Acceptors: Synergistic Bromine and Fluorine Substitution of the End Groups. *Adv. Mater.* **2024**, *36* (11), No. e2308216.
- (69) Chen, Y.; Yang, L.; Wu, J. L.; Wang, G.; Huang, W.; Melkonyan, F. S.; Lu, Z. Y.; Huang, Y.; Marks, T. J.; Facchetti, A. Performance, Morphology, and Charge Recombination Correlations in Ternary Squaraine Solar Cells. *Chem. Mater.* **2018**, *30* (19), 6810–6820.
- (70) Li, G.; Zhang, X.; Jones, L. O.; Alzola, J. M.; Mukherjee, S.; Feng, L. W.; Zhu, W.; Stern, C. L.; Huang, W.; Yu, J.; Sangwan, V. K.; DeLongchamp, D. M.; Kohlstedt, K. L.; Wasielewski, M. R.; Hersam, M. C.; Schatz, G. C.; Facchetti, A.; Marks, T. J. Systematic Merging of Nonfullerene Acceptor pi-Extension and Tetrafluorination Strategies Affords Polymer Solar Cells with > 16% Efficiency. *J. Am. Chem. Soc.* **2021**, *143* (16), 6123–6139.
- (71) Karki, A.; Vollbrecht, J.; Dixon, A. L.; Schopp, N.; Schrock, M.; Reddy, G. N. M.; Nguyen, T. Q. Understanding the High Performance of over 15% Efficiency in Single-Junction Bulk Heterojunction Organic Solar Cells. *Adv. Mater.* **2019**, *31* (48), No. e1903868.
- (72) Jiang, Y.; Liu, K.; Liu, F.; Ran, G.; Wang, M.; Zhang, T.; Xu, R.; Liu, H.; Zhang, W.; Wei, Z.; Cui, Y.; Lu, X.; Hou, J.; Zhu, X. 20.6% Efficiency Organic Solar Cells Enabled by Incorporating a Lower Bandgap Guest Nonfullerene Acceptor Without Open-Circuit Voltage Loss. *Adv. Mater.* **2025**, *37* (17), No. e2500282.
- (73) Liu, B.; Sun, H.; Lee, J. W.; Jiang, Z.; Qiao, J.; Wang, J.; Yang, J.; Feng, K.; Liao, Q.; An, M.; Li, B.; Han, D.; Xu, B.; Lian, H.; Niu, L.; Kim, B. J.; Guo, X. Efficient and stable organic solar cells enabled by multicomponent photoactive layer based on one-pot polymerization. *Nat. Commun.* **2023**, *14* (1), No. 967.
- (74) Wang, H. Q.; Zhong, Z. C.; Gámez-Valenzuela, S.; Lee, J. W.; Li, B. L.; Xu, C. J.; Yang, J.; Sun, H. L.; Kim, B. J.; Liu, B.; Guo, X. G. High-Performance Organic Solar Cells Enabled by 3D Globally Aromatic Carboranyl Solid Additive. *Adv. Funct. Mater.* **2025**, *35* (14), No. 2418805.
- (75) Blom, P. W. M.; deJong, M. J. M.; Vleggaar, J. J. M. Electron and hole transport in poly(p-phenylene vinylene) devices. *Appl. Phys. Lett.* **1996**, *68* (23), 3308–3310.
- (76) Hu, D.; Tang, H.; Chen, C.; Huang, P.; Shen, Z.; Li, H.; Liu, H.; Petoukhoff, C. E.; Jurado, J. P.; Luo, Y.; Xia, H.; Fong, P. W. K.; Fu, J.; Zhao, L.; Yan, C.; Chen, Y.; Cheng, P.; Lu, X.; Li, G.; Laquai, F.; Xiao, Z. Insights Into Preaggregation Control of Y-Series Nonfullerene Acceptors in Liquid State for Highly Efficient Binary Organic Solar Cells. *Adv. Mater.* **2024**, *36* (30), No. e2402833.
- (77) Zhu, J.; Zeng, R.; Zhou, E.; Li, C.; Deng, J.; Du, M.; Guo, Q.; Ji, M.; Wang, Z.; Lin, Y.; Han, F.; Zhuang, J.; Tan, S.; Kan, L.; Zhu, L.; Zhang, M.; Liu, F. A Refined Bulk P-I-N Structure in All-Polymer Solar Cells To Achieve 20.1% Efficiency and Improved Stability. *J. Am. Chem. Soc.* **2025**, *147* (28), 24491–24501.
- (78) Xu, Z.; Cao, X. J.; Yao, Z. Y.; Zhao, W. K.; Shi, W. D.; Bi, X. Q.; Li, Y.; Guo, Y. X.; Li, G. H.; Long, G. K.; Wan, X. J.; Li, C. X.; Chen, Y. S. Highly Efficient Acceptors with a Nonaromatic Thianthrene Central Core for Organic Photovoltaics. *Angew. Chem., Int. Ed.* **2025**, *64* (22), No. e202421289.
- (79) Pang, B.; Liao, C.; Xu, X.; Yu, L.; Li, R.; Peng, Q. Benzo[d]thiazole Based Wide Bandgap Donor Polymers Enable 19.54% Efficiency Organic Solar Cells Along with Desirable Batch-to-Batch Reproducibility and General Applicability. *Adv. Mater.* **2023**, *35* (21), No. e2300631.
- (80) Karki, A.; Vollbrecht, J.; Gillett, A. J.; Xiao, S. S.; Yang, Y.; Peng, Z.; Schopp, N.; Dixon, A. L.; Yoon, S.; Schrock, M.; Ade, H.; Reddy, G. N. M.; Friend, R. H.; Nguyen, T.-Q. The role of bulk and interfacial morphology in charge generation, recombination, and extraction in non-fullerene acceptor organic solar cells. *Energy Environ. Sci.* **2020**, *13* (10), 3679–3692.
- (81) Tian, G.; Li, Y.; Chen, Y.; Duan, T.; Hu, D.; Huang, P.; Chen, Q.; Liu, H.; Chen, H.; Lu, X.; Lu, S.; Xiao, Z. Relocating selenium alkyl chain enables efficient all-small molecule organic solar cells. *Chem. Eng. J.* **2024**, *482*, No. 149149.
- (82) Aldrich, T. J.; Matta, M.; Zhu, W.; Swick, S. M.; Stern, C. L.; Schatz, G. C.; Facchetti, A.; Melkonyan, F. S.; Marks, T. J. Fluorination Effects on Indacenodithienothiophene Acceptor Packing and Electronic Structure, End-Group Redistribution, and Solar Cell Photovoltaic Response. *J. Am. Chem. Soc.* **2019**, *141* (7), 3274–3287.
- (83) Liu, L.; Yu, F.; Hu, D.; Jiang, X.; Huang, P.; Li, Y.; Tian, G.; Lei, H.; Wu, S.; Tu, K.; Chen, C.; Gu, T.; Chen, Y.; Duan, T.; Xiao, Z. Breaking the symmetry of interfacial molecules with push–pull substituents enables 19.67% efficiency organic solar cells featuring enhanced charge extraction. *Energy Environ. Sci.* **2025**, *18* (4), 1722–1731.